Published in final edited form as:

Toxicol Pathol. 2018 January ; 46(1): 75–84. doi:10.1177/0192623317729222.

Repeated Iron-Soot Exposure and Nose-to-Brain Transport of Inhaled Ultrafine Particles

Laurie E. Hopkins[1,*], **Emilia A. Laing**[1,*], **Janice L. Peake**[1], **Dale Uyeminami**[1], **Savannah M. Mack**[1], **Xueting Li**[1,2], **Suzette Smiley-Jewell**[1], and **Kent E. Pinkerton**[1]

[1]Center for Health and the Environment, University of California, Davis, CA 95616

[2]Institute of Human Nutrition, Columbia University, New York, NY, 10032

Abstract

Particulate exposure has been implicated in the development of a number of neurological maladies, such as multiple sclerosis, amyotrophic lateral sclerosis, Alzheimer's disease, and idiopathic Parkinson's disease. Only a few studies have focused on the olfactory pathway as a portal through which combustion-generated particles may enter the brain. The primary objective of this study was to define the deposition, uptake, and transport of inhaled ultrafine iron-soot particles in the nasal cavities of mice to determine if combustion-generated nanoparticles reach the olfactory bulb via the olfactory epithelium and nerve fascicles. Adult female C57B6 mice were exposed to iron-soot combustion particles at a concentration of 200 μg/m³, which included 40 μg/m³ of iron-oxide nanoparticles. Mice were exposed for 6 hours per day, 5 days per week for 5 consecutive weeks (25 total exposure days). Our findings visually demonstrate that inhaled ultrafine iron-soot reached the brain via the olfactory nerves and was associated with indicators of neural inflammation.

Keywords

nose; brain; olfactory epithelium; ultrafine combustion particles; iron/soot

Introduction

There is a well-established association between exposure to particulate matter (PM) and numerous adverse cardiopulmonary health effects. Inhaled PM can readily cross the air-to-blood tissue barrier of the lungs with higher efficiency of systemic distribution as particle size decreases (Kreyling *et al.*, 2002). Particulate exposure has been implicated in the possible development of neurological conditions such as Alzheimer's and idiopathic Parkinson's (Gotz *et al.*, 2004, Kovacs, 2004, Linse *et al.*, 2007). Although extensive efforts have been directed towards understanding particle fate and cell-particle interactions in pulmonary and cardiovascular targets, those mechanisms and pathways through which inhaled PM may act on the central nervous system are just now becoming more fully

Corresponding author: Kent E. Pinkerton, Ph.D., Professor of Pediatrics, School of Medicine, Director, Center for Health and the Environment, University of California, Davis, kepinkerton@ucdavis.edu TEL: 530 752 8334.

*These authors contributed equally to this research

explored. PM may have enhanced entry to the brain from the systemic circulation by crossing the blood-to-brain endothelial barrier, perhaps via exposure-related changes in endothelial membrane permeability. Another possibility is PM may bypass the blood-brain barrier by entering the brain directly via uptake by olfactory sensory neurons (OSN), which have a direct connection to the olfactory epithelial lining of the nasal cavity with extension of their axons directly to the region of the olfactory bulb of the brain (Mombaerts, 2006).

Ambient particulates in polluted air can consist of a multifaceted mixture of highly diverse chemical entities, including hydrocarbons, sulfates, nitrates, metals, soot, and a combination of other organic and inorganic compounds (Kumar and Gill, 2009, Ngo *et al.*, 2010). Combustion-derived PM commonly contains transition metals, with iron being the predominant metal found in the ultrafine size fraction (Hughes and Cass, 1998). A leading hypothesis contends that exposure to transition metals, such as iron, elicits a pro-inflammatory response through redox cycling that is initially localized to sites of particle deposition, but may lead to a subsequent generalized inflammatory condition should the stimulus be sufficiently robust or persistent. If clearance of inhaled PM or nanoparticles is delayed, a chronic inflammatory condition could result. Such inflammatory processes of the brain are thought to play a central role in neurological dysfunction and disease (Cameron and Landreth, 2010, Chakraborty *et al.*, 2010, Czlonkowska and Kurkowska-Jastrzebska, 2011, Kim and Joh, 2006, Majde, 2010, Pott Godoy *et al.*, 2008).

The primary objective of this study was to define and visualize the uptake and transport of iron particles in the olfactory pathway. A secondary objective was to determine if the presence of iron-soot particles in the olfactory bulb would provoke an inflammatory response. To accomplish these goals, an iron-soot combustion particle aerosol was experimentally generated at a concentration of 200 μg/m³, including 40 μg/m³ of iron nanoparticles, using a laminar diffusion flame system. Exposure of mice to this aerosol took place for 6 h/day, 5 days/week, for a total of 5 weeks (25 exposure days).

Materials and Methods

Animals

Thirty-six adult female C57B6 mice (23 ± 1.2 g body weight) nine weeks of age at the onset of experimental exposure were purchased from Charles River Labs (Wilmington, MA). Mice were randomly assigned to two exposure groups (iron-soot, n=24; filtered air, n=12) and allowed to acclimate for at least one week prior to the onset of experimental exposures. Mice were housed, up to four per cage, in filter-top polycarbonate cages in an animal facility with high-efficiency particulate air filters. Except during the actual period of exposure, mice were allowed water and a standard laboratory mouse diet *ad libitum*. All animals were handled in accordance with guidelines established by the Institutional Animal Care and Use Committee (IAUCAC) of the University of California, Davis.

Inhalation exposures

Mice were housed in sealed 20 cm × 43 cm × 18 cm polycarbonate whole-body chambers during exposure to an aerosol of ultrafine iron-soot at a target concentration of 200 μg/m^3,

including 40 μg/m^3 of iron-oxide nanoparticles. The total soot-iron aerosol generated was cooled and diluted with filtered air to achieve the desired concentration prior to reaching the exposure chambers. Mice were exposed 6 hours/day, 5 days/week for 5 consecutive weeks (25 total exposure days). The sham-control group was exposed to filtered air only. Flow rate through the whole-body exposure chambers was 7 L/min for a total air exchange of 2.2/min or 133/hour. Chamber ozone and CO_2 levels were not detected, while oxides of nitrogen were below 0.1 ppm. Chamber temperature averaged 68–70°F. During each exposure period, the animals were unrestrained and allowed to engage in normal activity, although access to food and water was denied.

Generation and characterization of particles

Particles were generated in a laminar diffusion flame system using ethylene gas as the primary hydrocarbon fuel mixed with acetylene gas to compensate for the effect of iron-oxide to suppress soot formation (Fig. 1). The source of iron was iron pentacarbonyl vaporized from a liquid reservoir warmed to 20°C with an argon carrier gas (all Sigma-Aldrich Chemical Co., St. Louis, MO) combusted in the presence of an ethylene/acetylene vapor mix. Combustion of these reactants generated a hetero-disperse aerosol of ultrafine iron oxide particles (Fe_2O_3) and associated soot. A detailed description of the system and the particles generated is available (Jasinski *et al.*, 2006, Pinkerton *et al.*, 2008, Yang *et al.*, 2001). A target particle concentration of 200 μg/m^3 was selected to simulate unhealthy air quality conditions, while remaining at a concentration of particulate emissions that would be reminiscent of heavy pollution days seen with wildfires in the United States in recent years, as well as poor air quality days experienced today in many parts of the world including China (Pui *et al.,* 2014, Connor, 2015). A scanning mobility size analyzer (SMPS 3936, TSI, Shoreview, MN) was run concurrently during animal exposure to determine particle size distribution. These data were collected to determine whether the desired size and target concentration were achieved and to provide a measure of uniformity of exposure during the course of the experiment. Aerosol was collected daily on 25 mm Teflon-coated filters (Teflo Pall, East Hills, NY) of 3.0 μm pore size and sent to an independent laboratory (Chester Labnet, Tigard, OR) for metal analysis by x-ray fluorescence (XRF) to determine iron content. Total mass concentration data was obtained gravimetrically by weighing 25 mm Pallflex Emfab filters (VMR International, Radnor, PA) on a microbalance before and after sample collection. Samples for TEM particle visualization were collected on 3 mm carbon-coated (‘lacey carbon’) copper grids using a point-to-plane electrostatic precipitator.

Tissue collection

Twenty-four hours following the final exposure day, mice were deeply anesthetized by an intraperitoneal injection of sodium pentobarbital anesthetic (65 mg/g body weight) (Nembutal, Cardinal Health, Sacramento, CA) diluted 1:6 with phosphate-buffered saline solution at 1 mg/kg body weight, e.g., 0.03 cc for a 30 g mouse. A total of 32 mice were used for histological and protein analysis (12 control and 20 exposed).

Fixed tissue: Nasal cavity, olfactory bulb and brain—When complete sedation was achieved (i.e., the mouse was unresponsive to toe pinch test), the thorax was opened and the lungs inflated to 18 psi via cannulation of the trachea. Whole-body fixation was achieved by

vascular perfusion with heparinized phosphate buffered saline (USP grade) followed by 4% paraformaldehyde. The cannula for perfusion was placed into the right ventricular chamber with flow directed toward the pulmonary valve and trunk and outflow through the jugular vein. Perfusion-fixed tissues were harvested and immersed in 4% paraformaldehyde until further processing for histological analyses. The cranium was opened along the dorsal midline to remove the brain olfactory bulb, taking care to minimize stretching of the olfactory nerves. Nasal cavities were gently flushed in a retrograde manner with fixative using a syringe inserted into the exposed end of the trachea. Retrograde perfusion was done to ensure that fixative exited both nares, indicating complete flushing of the nasal cavity. The lower jaw was removed, and the head cleaned of skin and superficial muscles. Trimmed heads were immersed in fixative for at least 24 hours prior to demineralization in 10% EDTA solution (Immunocal, American MasterTech, Lodi, CA), followed by further trimming, slicing of the nasal cavity and eventual embedment in Paraplast (Fisher Scientific, Swedesboro, NJ).

Unfixed tissue: Olfactory bulb and brain—Mice were killed by decapitation using a guillotine after complete sedation (verified by toe pinch test), and the brain was immediately removed in the manner described above. Olfactory bulbs were processed and analyzed separately from other portions of the brain. Homogenates of the olfactory bulb were prepared for protein analysis.

Histologic preparation of the nasal cavity, olfactory bulb and brain – staining methodology

When preparing and cutting the nasal cavity, olfactory bulb, and brain for embedment in Paraplast, care was taken to avoid particle transfer; each cut was made with a fresh blade in a caudal-to-rostral direction. Sagittal sections of nasal cavities were cut using a microtome to a thickness of 5 μm, while the brain and olfactory bulb tissues were serially sectioned to 10 μm. Within the nasal cavity, step series at 50 μm intervals were taken for identification of the olfactory epithelium and nerve bundles within the nasal cavity, along with the localization of ferric iron within neural and olfactory tissues. Microglial cells within the olfactory bulb were visualized using Ricinus communis agglutinin lectin (RCA-1), which strongly binds to microglial cells to categorize both resting and activated forms of the cell (Wierzba-Bobrowicz *et al.,* 1997).

Ferric iron visualization

Iron was visualized directly in fixed, paraffin embedded sections of nasal cavity, brain, and olfactory bulb by staining with Prussian blue, a standard histologic method of detecting iron in tissue in which ferric iron interacts with potassium ferrocyanide to form ferric ferrocyanide, a deep blue precipitate. Only the insoluble form of iron, ferric iron (Fe +++), is labeled by this technique. Neutral red was used as a counterstain to visualize nuclei and to lightly stain surrounding structures. A complete series of step sections of the olfactory bulb at 50 μm intervals were collected.

Olfactory and microglial cell visualization

Staining with hematoxylin and eosin (H&E) was used to visualize the anatomy and composition of the nasal cavity, olfactory bulb and brain. Sections of the nasal cavity were

also stained with protein gene product 9.5 (PGP9.5), a general nerve marker (Pinkerton and Joad, 2006) antibody specific for olfactory epithelium, nerves and nerve fascicles. Microglial cells in sections of the olfactory bulb tissue were visualized using RCA-1 staining (Vector Labs, Burlingame, CA) as per a modified method of Hauke and Korr (Hauke and Korr, 1993). Briefly, tissue sections were deparaffinized, incubated with RCA-1 lectin followed by 3,3′-diaminobenzidine (DAB) chromogen + substrate (Dako North America, Carpinteria, CA) and counterstained with hematoxylin. Antigen retrieval using hydrogen peroxide was implemented to increase binding sites to achieve strong, specific labeling with low background and adequate contrast to view cell morphology in 10 μm thick sections.

RCA-1 binds to β-D-galactose moieties present on microglial cells, epithelial cells, and vascular endothelial cells, which are easily differentiated on the basis of their morphology. Microglial cells exhibit a range of morphological conformations correlating with activation state, presenting a gradient from resting to fully activated (Colton and Wilcock, 2010, Lawson *et al.*, 1990, Stence *et al.*, 2001). Microglial cells were counted in two histological sections per animal for six animals per exposure group. All microglial cells were counted in each of six non-overlapping fields per section and classified as either resting or activated using pre-determined criteria based on Stence's characterization of ramified versus motile stages (Stence *et al.*, 2001). Criteria for microglial cell categorization as 'resting' included strong RCA-1 lectin positive staining and at least two highly branched (ramified) processes extending at least twice the length of a highly elliptical (flattened) nucleus. Criteria for microglial cell categorization as 'activated' included strong RCA-1 lectin positive staining and no more than two visible processes of more than half the length of the large roughly circular nucleus or large overall size and amoeboid shape accompanied by dense staining. RCA-1 positive cells not meeting either set of criteria (i.e., intermediate forms) were excluded from counting. Two levels of the olfactory bulb were analyzed with 6 fields per level using a 20X objective lens for a total of 12 non-overlapping fields. A total of 6 animals from each group were examined. Activated and resting microglial cells were counted for each animal. The ratio of activated to resting microglial cells was also determined.

Preparation of tissue homogenates

Olfactory bulb homogenates were prepared from unfixed frozen tissues placed in flat-bottom tubes (Eppendorf North America, Hauppauge, NY) containing stainless steel balls, lysis buffer (Pierce Protein Research, Thermo Fisher Scientific, Waltham, MA), protease inhibitor cocktail (Complete, Roche Diagnostics, Indianapolis, IN), and sonicated for four minutes at 20 Hertz in a Qiagen TissueLyser (Qiagen Inc., USA, Valencia, CA). Aliquots were stored on ice until cytokine and total protein content analyses.

BCA protein assay

Total protein in olfactory bulb homogenates was determined using a commercially available BCA protein assay kit (Pierce Protein Research) in accordance with the manufacturer's instructions for a 96-well plate micro-assay. Assays were read on a BioTek Synergy2 plate reader with Gen5 software (BioTek Instruments, Winooski, VT).

ELISA for cytokines

Levels of the pro-inflammatory cytokines TNF α and IL-1β were analyzed in olfactory bulb homogenates using commercial ELISA kits (Cell BioLabs, San Diego, CA; R&D Systems Inc., Minneapolis, MN, respectively). Homogenates were diluted as necessary to achieve the protein concentration recommended by each ELISA kit manufacturer. However, due to the small size of the mouse olfactory bulbs collected, the volume of tissue homogenate available for these assays was limited and precluded the use of a more concentrated sample for analysis of TNF α on a per mouse basis.

Statistical analysis

For quantitative endpoints (cytokine expression, microglial cell counts), mean values per exposure group were determined and expressed ± standard deviation. Data were analyzed using Excel (Microsoft Corporation, Redmond, WA). Student's *t* test was performed on group mean values, with significance accepted at $p \leq 0.05$.

Results

Ultrafine iron-soot aerosol characterization

Particle size distribution remained consistent between samples taken daily during the exposure. Average total suspended particle mass concentration for the 25 exposure days was 203 ± 13 μg/m^3, of which an average 38 μg/m^3 was composed of iron. Daily median particle diameter ranged from 44 nm to 59 nm; the 25-day average was 50.4 ± 4 nm.

Identification of olfactory epithelium and pathways to the olfactory bulb and brain

PGP9.5 staining of transverse sections through the nasal cavity (Fig. 4) demonstrates the extensive distribution of the olfactory epithelium and nerve fascicles throughout the rostral portions of the nasal cavity, in particular in both posterior and apical regions. A sagittally-cut tissue section through the posterior region of the nasal cavity stained with H&E (Fig. 5) shows in a single plane the relative position of the olfactory epithelium to the nerve fascicles that pass through the cribriform plate to the olfactory bulb (Fig. 5). This plane of section also allows for the visualization of the glomerular and external plexiform layers the olfactory bulb where the individual olfactory nerve axons synapse with the olfactory bulb (Fig. 5).

Visualization of iron in olfactory tissues and nerves

Prussian blue reaction product, indicative of the presence of ferric iron, was found abundantly in the olfactory nerve fascicles leading to the olfactory bulb of iron-soot combustion particle exposed mice (Fig. 6). Prussian blue staining was not noted in the sham-exposed controls (data not shown). Occasional strong punctate iron-positive staining of olfactory nerve fascicles exiting the olfactory epithelium was noted in route to the olfactory bulbs with small foci of iron accumulation within the olfactory bulbs observed (Fig. 7). Iron distribution was not completely uniform; only a few of the olfactory nerve fascicles in any given tissue section were iron-positive. In addition, it was noted in some nerve fascicles, that the iron appeared to be limited to the outer layers of the nerve bundle (Fig. 6B). Specific regions of the olfactory bulb in mice exposed to iron-soot were stained iron-positive,

primarily in the posterior portion of the bulb, near the boundary of the accessory olfactory bulb. Iron-laden cells also were occasionally observed in these posterior regions of the bulb. Iron staining in the apical region of the olfactory epithelium was only occasionally observed and always in a fine punctate manner.

Microglial cells and markers of inflammation in the olfactory bulb

Microglial cells and the endothelium/smooth muscle of blood vessels stained positively for RCA-1 lectin (Fig. 8). Resting microglia were visualized as thin, elongated extensions of cytoplasm between neural cells, while activated microglia possessed short, stubby elongated processes close to the centrally-located nucleus.

The total number of microglial cells (activated and resting) per unit area of the olfactory bulb did not significantly change between sham control animals and animals exposed to ultrafine iron-soot particles (Fig. 9). In contrast, the ratio of activated to resting microglial cells was significantly greater in mice exposed to iron-soot in contrast to that observed in sham controls (0.47 vs. 0.39; $p = 0.045$) (Fig. 10).

The level of the pro-inflammatory cytokine IL-1β in olfactory bulb homogenates from iron-soot-exposed mice was significantly greater compared to IL-1β measured in sham control mice (Fig. 11). In contrast, TNF α levels were near or below the detection limit of the assay in both exposure groups (data not shown).

Discussion

The primary objective of this study was to detect the deposition, uptake, and transport of inhaled ultrafine iron-soot particles via the olfactory pathway to the brain. Although particles may reach the brain via other pathways, nose-to-brain transport of metals has been reported in a limited number of studies. With rare exceptions, the method of exposure in these studies was by intranasal instillation of ionic forms of the particle. More recent studies of nose-to-brain delivery of engineered nanoparticles for therapeutic goals also in general apply intranasal instillation as the preferred method of administration. Recent research further exploring the potential toxic effects of nanoparticles reaching the brain is still developing (Ahmad *et al.*, 2016, Gao, 2016, Hao *et al.*, 2016, Muntimadugu *et al.*, 2016) although the actual passage of these particles has not been visualized.

Setting aside the question of how well intranasal delivery of a bolus of particles substitutes for exposure by inhalation to an aerosol, the data presented as evidence of olfactory sensory neuron-mediated transport continue to be suggestive, circumstantial and not absolutely confirmatory (Doty, 2008, Mistry *et al.*, 2009, Oberdorster *et al.*, 2004, Rao *et al.*, 2003). In these published studies, translocated particles are presumed to have reached the brain by way of olfactory axonal tracts despite the paucity of direct evidence to support the assumption. The current study supplies this evidence by visually demonstrating olfactory nerve uptake of iron using Prussian blue staining.

Although nerve fascicles arising from the olfactory epithelium demonstrated the uptake of iron by way of Prussian blue staining, abundant iron-positive staining within the glomerular

layer of the olfactory bulb was not observed in histological sections. In contrast, iron as visualized by Prussian blue staining was found distributed in the deeper layers of the olfactory bulb. This observation might suggest iron found in the olfactory bulb could have arrived by way of the systemic circulation. Much of the aerosol in these inhalation exposures reached the lung (data not published). Most particles deposited in pulmonary regions are cleared via the mucociliary escalator and subsequently swallowed. Some bioavailable iron has been identified in the aerosols generated in our combustion particle system (Pinkerton *et al.*, 2008). Thus, it is possible that some iron may have been taken up from the lung or the gut with iron in the blood entering the brain by crossing vascular endothelial membranes.

In general, movement of iron in the body is tightly regulated. However, when inflammation is present there may be changes in the movement of iron across the blood-brain barrier due to increased vascular permeability (Shaftel *et al.*, 2007, Thornton *et al.*, 2010). However, we believe this is not the primary route for entry of iron to the olfactory bulb and brain in this study for several reasons: (1) the pro-inflammatory response observed was not pronounced, (2) there is strong evidence of iron in the olfactory nerve tracts linking the nasal mucosa to the olfactory bulb, and (3) foci of iron accumulation are found in the olfactory bulb but not elsewhere in the brain. A study from our laboratory showed nose-to-brain transport of aerosolized quantum dots, a form of semiconductor nanocrystal, in mice occurred with significant activation of microglial cells (Hopkins *et al.*, 2014). This study, although not comprehensive, demonstrated the presence of quantum dots along axonal pathways by transmission electron microscopy, as well as fluorescent detection of quantum dots in unfixed olfactory bulb preparations. Similarly, silver nanoparticles were found transported to the olfactory bulb of rats, also demonstrating microglial cell activation (Patchin *et al.*, 2016). A recent article reviewed a number of papers in the literature in which olfactory nerve transport was observed (Heusinkveld *et al.*, 2016). While we acknowledge there are other pathways through which ultrafine particles may reach the brain, the primary purpose of this study was to verify that ultrafine particles found in combustion emissions can be transported to the brain via the olfactory route.

Although the lung is a primary site for the deposition of inhaled ultrafine particles, there is also a high level of deposition of ultraparticles in the nasal cavity as well. The current study suggests the upper respiratory tract contributes in a different, but significant fashion to total brain uptake, highlighting the potential for multiplicity of particle effects by particles acting on different targets concurrently. Our results demonstrate increased microglial cell activation and neural inflammation. Zhong et al. also noted significant pro-inflammatory responses to the same ultrafine iron-soot material at higher exposure concentrations (Zhong *et al.*, 2010, Zhou *et al.*, 2003b) and at lower concentrations comparable to those used in this study to cause significant synergistic effects of iron-soot exposure (Zhong *et al.*, 2010, Zhou *et al.*, 2003a). In this study, we opted to not use higher concentrations of iron to create what we felt would be an environmentally relevant level of metals within our iron-soot combustion particulate emission system delivered to the nose and rest of the respiratory tract via inhalation.

In summary, this study confirms inhaled ultrafine iron oxide can reach the brain via olfactory nerve fascicles. Evidence of inflammatory changes in the olfactory bulb following exposure

to ultrafine iron-soot particles provides further support to the concept that long-term exposure to ambient PM may play a role in neurological disease in humans. In addition, as nanoparticles continue to be developed to treat neurological diseases, it is important to take into consideration possible pro-inflammatory changes in the CNS that these particles could elicit. The combined effect of concurrent particle-related responses in multiple targets, such as the lung and the olfactory bulb, could lead to a generalized adverse impact on the health of susceptible individuals. It may be the case that long-term exposure to low levels of ultrafine particulate matter results in a chronic inflammatory state, a condition associated with chronic disease in humans. As speculation that exposure to airborne particles might be a causative agent in neurodegenerative disorders continues to grow, further investigation of the olfactory pathway as a port of entry is warranted.

Acknowledgments

This research was supported by the National Institute of Environmental Health Sciences (U01ES027288, P30ES023513), the National Institute for Occupational Safety and Health (US4 0H07550), and the National Institute of Health (P51 OD011107). We thank the Western Center for Agricultural Health and Safety and the Environmental Health Science Core Center at the University of California, Davis for services provided to make this research possible.

References

Ahmad N, Ahmad R, Naqvi AA, Alam MA, Ashafaq M, Samim M, Iqbal Z and Ahmad FJ (2016). Rutin-encapsulated chitosan nanoparticles targeted to the brain in the treatment of Cerebral Ischemia. International journal of biological macromolecules, 91, 640–655. [PubMed: 27264648]

Cameron B and Landreth GE (2010). Inflammation, microglia, and Alzheimer's disease. Neurobiology of disease, 37, 503–509. [PubMed: 19833208]

Chakraborty S, Kaushik DK, Gupta M and Basu A (2010). Inflammasome signaling at the heart of central nervous system pathology. Journal of neuroscience research, 88, 1615–1631. [PubMed: 20127816]

Colton C and Wilcock DM (2010). Assessing activation states in microglia. CNS & neurological disorders drug targets, 9, 174–191. [PubMed: 20205642]

Connor N (2015). Choking smog more than 50 times health guidelines blankets China. The Telegraph, 9 11 2015.

Czlonkowska A and Kurkowska-Jastrzebska I (2011). Inflammation and gliosis in neurological diseases--clinical implications. Journal of neuroimmunology, 231, 78–85. [PubMed: 20943275]

Doty RL (2008). The olfactory vector hypothesis of neurodegenerative disease: is it viable? Annals of neurology, 63, 7–15. [PubMed: 18232016]

Gao H (2016). Progress and perspectives on targeting nanoparticles for brain drug delivery. Acta pharmaceutica Sinica. B, 6, 268–286. [PubMed: 27471668]

Gotz J, Schild A, Hoerndli F and Pennanen L (2004). Amyloid-induced neurofibrillary tangle formation in Alzheimer's disease: insight from transgenic mouse and tissue-culture models. International journal of developmental neuroscience : the official journal of the International Society for Developmental Neuroscience, 22, 453–465. [PubMed: 15465275]

Hao J, Zhao J, Zhang S, Tong T, Zhuang Q, Jin K, Chen W and Tang H (2016). Fabrication of an ionic-sensitive in situ gel loaded with resveratrol nanosuspensions intended for direct nose-to-brain delivery. Colloids and surfaces. B, Biointerfaces, 147, 376–386. [PubMed: 27566226]

Hauke C and Korr H (1993). RCA-I lectin histochemistry after trypsinisation enables the identification of microglial cells in thin paraffin sections of the mouse brain. Journal of neuroscience methods, 50, 273–277. [PubMed: 7512170]

Heusinkveld HJ, Wahle T, Campbell A, Westerink RH, Tran L, Johnston H, Stone V, Cassee FR and Schins RP (2016). Neurodegenerative and neurological disorders by small inhaled particles. Neurotoxicology, 56, 94–106. [PubMed: 27448464]

Hopkins LE, Patchin ES, Chiu PL, Brandenberger C, Smiley-Jewell S and Pinkerton KE (2014). Nose-to-brain transport of aerosolised quantum dots following acute exposure. Nanotoxicology, 8, 885–893. [PubMed: 24040866]

Hughes LS and Cass GR (1998). Physical and Chemical Characterization of Atmospheric Ultrafine Particles in the Los Angeles Area. Environmental Science & Technology, 32, 1153–1161.

Jasinski J, Pinkerton KE, Kennedy IM and Leppert VJ (2006). Spatially resolved energy electron loss spectroscopy studies of iron oxide nanoparticles. Microscopy and microanalysis : the official journal of Microscopy Society of America, Microbeam Analysis Society, Microscopical Society of Canada, 12, 424–431.

Kim YS and Joh TH (2006). Microglia, major player in the brain inflammation: their roles in the pathogenesis of Parkinson's disease. Experimental & molecular medicine, 38, 333–347. [PubMed: 16953112]

Kovacs T (2004). Mechanisms of olfactory dysfunction in aging and neurodegenerative disorders. Ageing research reviews, 3, 215–232. [PubMed: 15177056]

Kreyling WG, Semmler M, Erbe F, Mayer P, Takenaka S, Schulz H, Oberdorster G and Ziesenis A (2002). Translocation of ultrafine insoluble iridium particles from lung epithelium to extrapulmonary organs is size dependent but very low. Journal of toxicology and environmental health. Part A, 65, 1513–1530. [PubMed: 12396866]

Kumar V and Gill KD (2009). Aluminium neurotoxicity: neurobehavioural and oxidative aspects. Archives of toxicology, 83, 965–978. [PubMed: 19568732]

Lawson LJ, Perry VH, Dri P and Gordon S (1990). Heterogeneity in the distribution and morphology of microglia in the normal adult mouse brain. Neuroscience, 39, 151–170. [PubMed: 2089275]

Linse S, Cabaleiro-Lago C, Xue WF, Lynch I, Lindman S, Thulin E, Radford SE and Dawson KA (2007). Nucleation of protein fibrillation by nanoparticles. Proceedings of the National Academy of Sciences of the United States of America, 104, 8691–8696. [PubMed: 17485668]

Majde JA (2010). Neuroinflammation resulting from covert brain invasion by common viruses - a potential role in local and global neurodegeneration. Medical hypotheses, 75, 204–213. [PubMed: 20236772]

Mistry A, Stolnik S and Illum L (2009). Nanoparticles for direct nose-to-brain delivery of drugs. International journal of pharmaceutics, 379, 146–157. [PubMed: 19555750]

Mombaerts P (2006). Axonal wiring in the mouse olfactory system. Annual review of cell and developmental biology, 22, 713–737.

Muntimadugu E, Dhommati R, Jain A, Challa VG, Shaheen M and Khan W (2016). Intranasal delivery of nanoparticle encapsulated tarenflurbil: A potential brain targeting strategy for Alzheimer's disease. European journal of pharmaceutical sciences : official journal of the European Federation for Pharmaceutical Sciences, 92, 224–234. [PubMed: 27185298]

Ngo MA, Pinkerton KE, Freeland S, Geller M, Ham W, Cliff S, Hopkins LE, Kleeman MJ, Kodavanti UP, Meharg E, Plummer L, Recendez JJ, Schenker MB, Sioutas C, Smiley-Jewell S, Haas C, Gutstein J and Wexler AS (2010). Airborne particles in the San Joaquin Valley may affect human health. California Agriculture, 64, 12–16.

Oberdorster G, Sharp Z, Atudorei V, Elder A, Gelein R, Kreyling W and Cox C (2004). Translocation of inhaled ultrafine particles to the brain. Inhalation toxicology, 16, 437–445. [PubMed: 15204759]

Patchin ES, Anderson DS, Silva RM, Uyeminami DL, Scott GM, Guo T, Van Winkle LS and Pinkerton KE (2016). Size-Dependent Deposition, Translocation, and Microglial Activation of Inhaled Silver Nanoparticles in the Rodent Nose and Brain. Environmental health perspectives, 124, 1870–1875. [PubMed: 27152509]

Pinkerton KE and Joad JP (2006). Influence of air pollution on respiratory health during perinatal development. Clinical and experimental pharmacology & physiology, 33, 269–272. [PubMed: 16487273]

Pinkerton KE, Zhou Y, Zhong C, Smith KR, Teague SV, Kennedy IM and Menache MG (2008). Mechanisms of particulate matter toxicity in neonatal and young adult rat lungs. Research report (Health Effects Institute), 3–41; discussion 43–52. [PubMed: 19203021]

Pott Godoy MC, Tarelli R, Ferrari CC, Sarchi MI and Pitossi FJ (2008). Central and systemic IL-1 exacerbates neurodegeneration and motor symptoms in a model of Parkinson's disease. Brain : a journal of neurology, 131, 1880–1894. [PubMed: 18504291]

Pui DYH, Chen SC, and Zuo Z (2014). $PM_{2.5}$ in China: Measurements, sources, visibility and health effects, and mitigation. Particuology, 13, 1–26.

Rao DB, Wong BA, McManus BE, McElveen AM, James AR and Dorman DC (2003). Inhaled iron, unlike manganese, is not transported to the rat brain via the olfactory pathway. Toxicology and applied pharmacology, 193, 116–126. [PubMed: 14613722]

Shaftel SS, Carlson TJ, Olschowka JA, Kyrkanides S, Matousek SB and O'Banion MK (2007). Chronic interleukin-1beta expression in mouse brain leads to leukocyte infiltration and neutrophil-independent blood brain barrier permeability without overt neurodegeneration. The Journal of neuroscience : the official journal of the Society for Neuroscience, 27, 9301–9309. [PubMed: 17728444]

Stence N, Waite M and Dailey ME (2001). Dynamics of microglial activation: a confocal time-lapse analysis in hippocampal slices. Glia, 33, 256–266. [PubMed: 11241743]

Thornton P, McColl BW, Cooper L, Rothwell NJ and Allan SM (2010). Interleukin-1 drives cerebrovascular inflammation via MAP kinase-independent pathways. Current neurovascular research, 7, 330–340. [PubMed: 20854249]

Wierzba-Bobrowicz T, Lechowicz W, and Kosno-Kruszewska E (1997). A morphometric evaluation of morphological types of microglia and astroglia in human fetal mesencephalon. Folia Neuropathologica, 35, 29–35. [PubMed: 9161098]

Yang GS, Teague S, Pinkerton K and Kennedy IM (2001). Synthesis of an ultrafine iron and soot aerosol for the evaluation of particle toxicity. Aerosol Science and Technology, 35, 759–766.

Zhong CY, Zhou YM, Smith KR, Kennedy IM, Chen CY, Aust AE and Pinkerton KE (2010). Oxidative injury in the lungs of neonatal rats following short-term exposure to ultrafine iron and soot particles. Journal of toxicology and environmental health. Part A, 73, 837–847. [PubMed: 20391124]

Zhou YM, Zhong CY, Kennedy IM, Leppert VJ and Pinkerton KE (2003a). Oxidative stress and NFkappaB activation in the lungs of rats: a synergistic interaction between soot and iron particles. Toxicology and applied pharmacology, 190, 157–169. [PubMed: 12878045]

Zhou YM, Zhong CY, Kennedy IM and Pinkerton KE (2003b). Pulmonary responses of acute exposure to ultrafine iron particles in healthy adult rats. Environmental toxicology, 18, 227–235. [PubMed: 12900941]

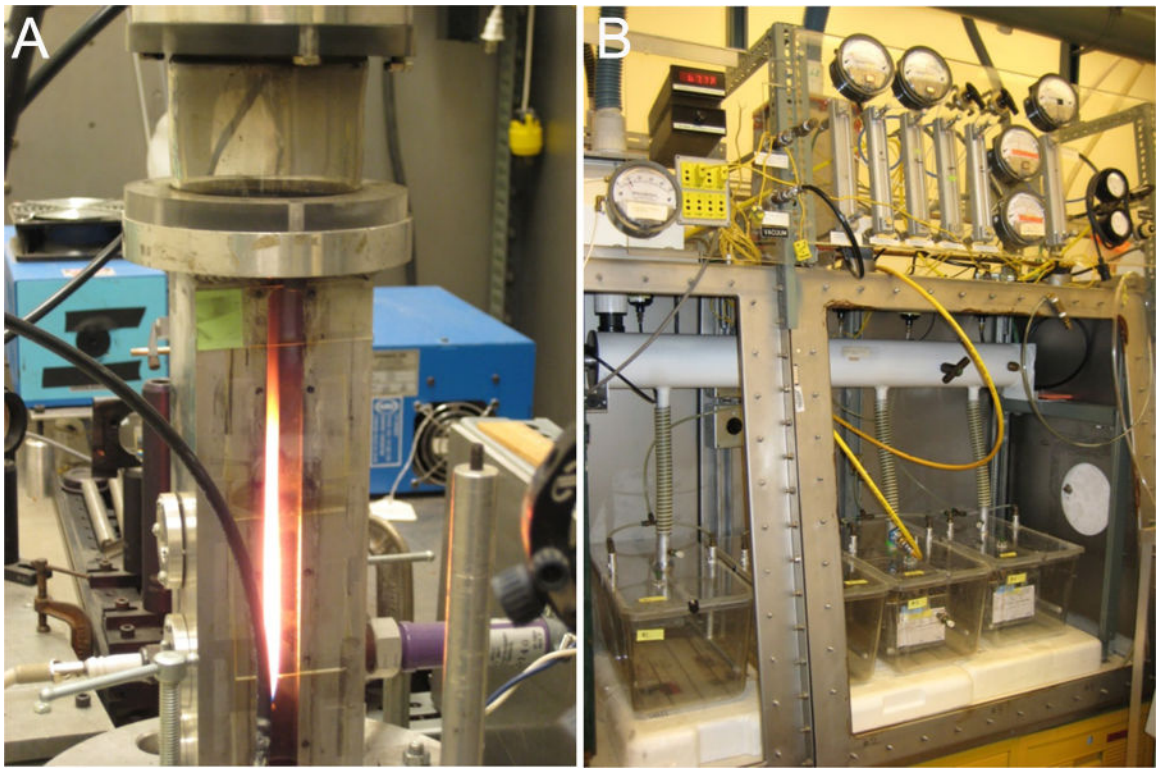

Figure 1.

(A) Laminar diffusion flame system used to generate ultrafine iron oxide and soot particles. (B) Whole-body exposure chambers designed to deliver a constant stable concentration of total iron–soot combustion particles for 6 hr/day, 5 days/week for a total of 5 weeks.

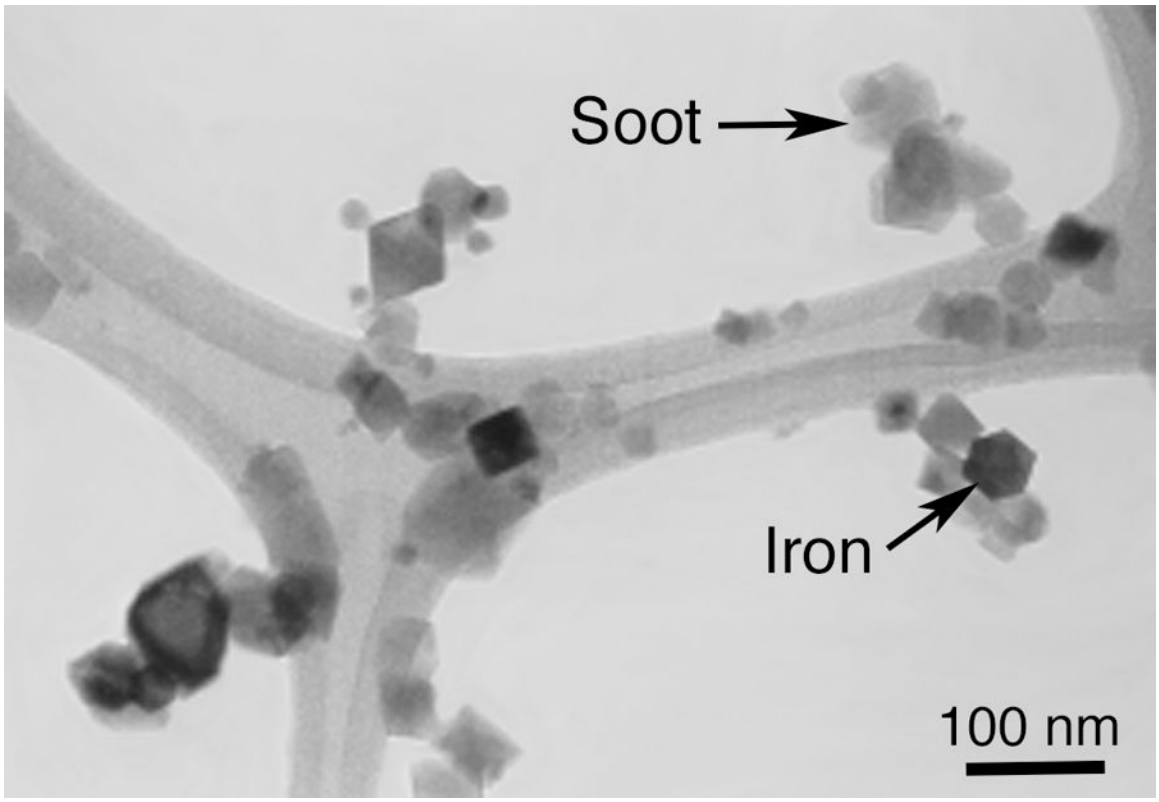

Figure 2.
Transmission electron micrograph of iron–soot particles collected on a carbon-coated holey grid.

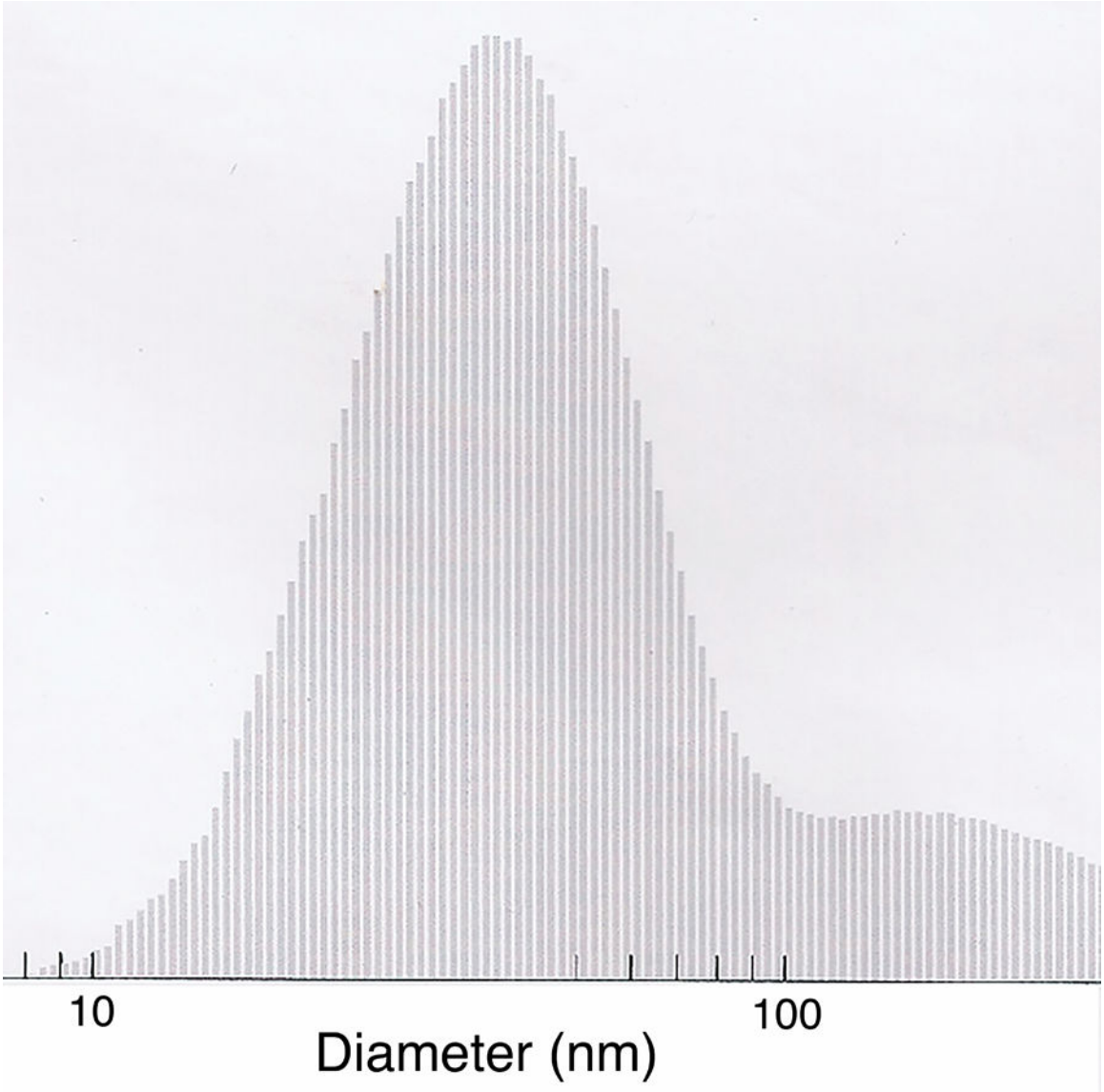

Figure 3.
Histogram of nanoparticle size as measured by a scanning mobility particle sizer with a mean particle size of 50 + 4 nm.

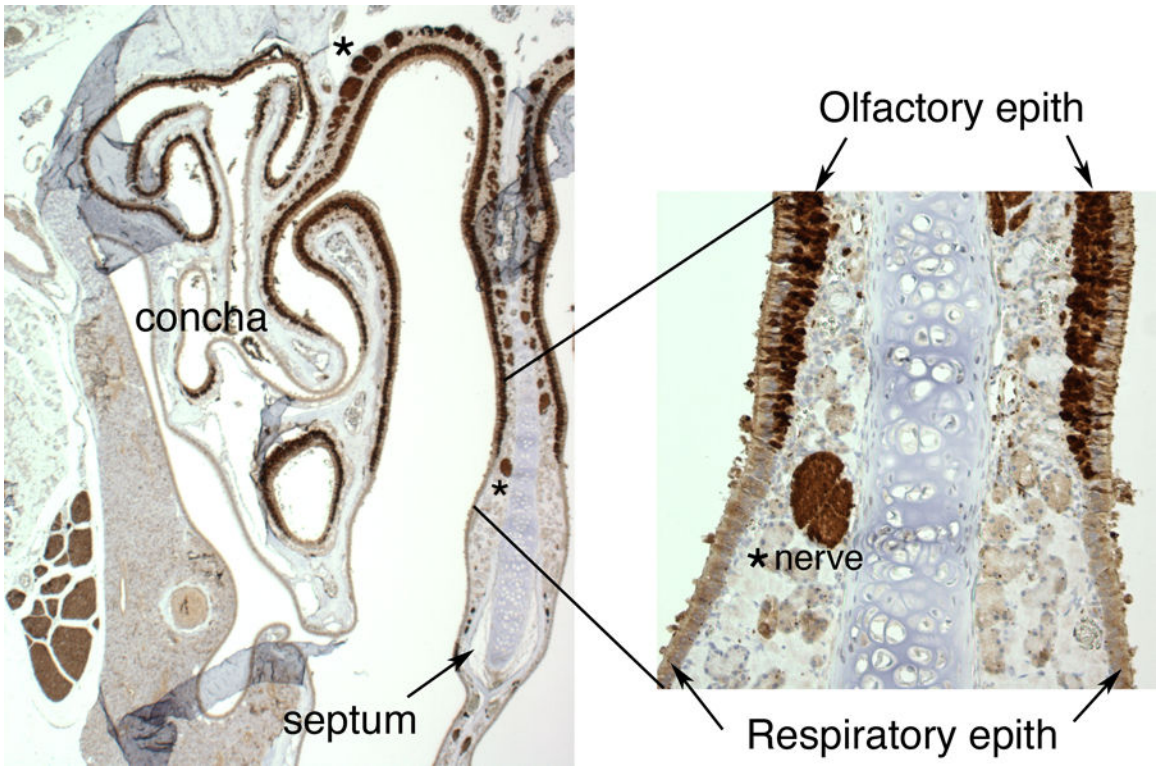

Figure 4.

Cross-sectional view of the murine nasal cavity stained with protein gene product 9.5, a general nerve marker, to visualize neural positive tissues and cells, including the olfactory epithelium, nerves, and nerve bundles. The region shown includes the upper portions of the caudal region of the nasal cavity with clearly marked regions of olfactory epithelium and underlying nerves.

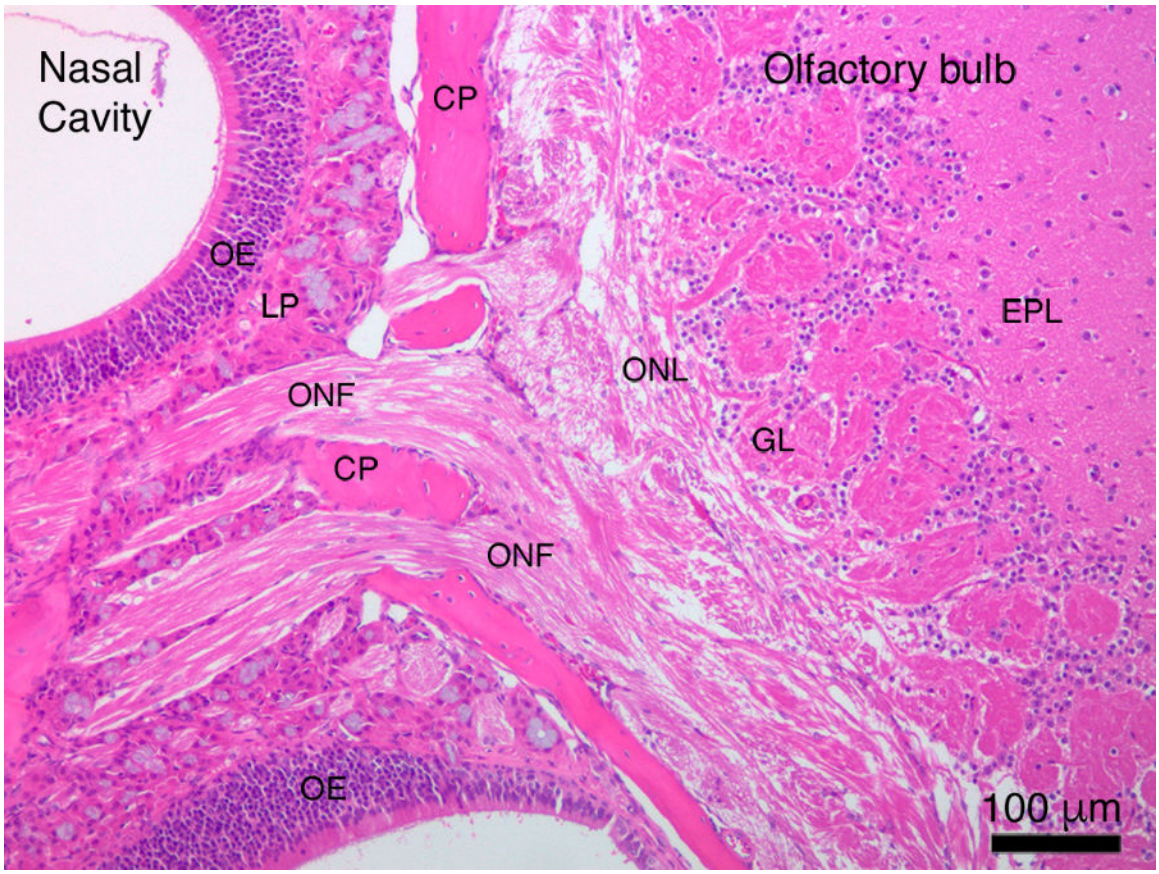

Figure 5.

Direct visualization of the neural pathway from the nasal cavity to the olfactory bulb of the brain. CP ¼ cribriform plate; EPL ¼ external plexiform layer; GL ¼ glomerular layer; LP ¼ lamina propria; OE ¼ olfactory epithelium; ONF ¼ olfactory nerve fascicle; ONL ¼ olfactory nerve layer.

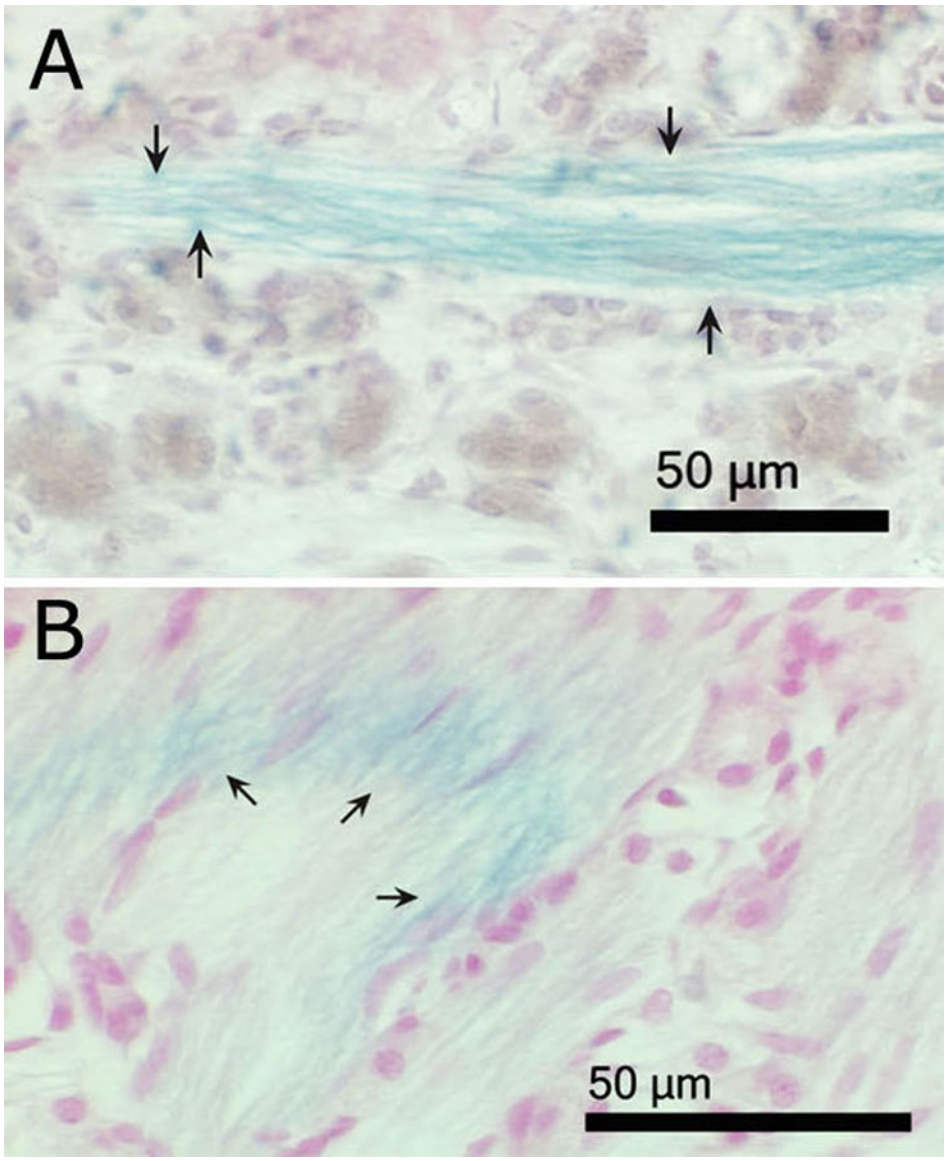

Figure 6.

Light micrographs of paraffin sections of nasal cavities from iron–soot exposed mice, showing the lamina propria region of olfactory mucosa. (A) The plane of section is roughly parallel to the fascicle. (B) The plane of section cuts across several nerve fascicles at an oblique angle, producing an elliptical cross section. Arrows indicate Prussian blue-positive olfactory nerve fibers, demonstrating the presence of ferric iron. Tissues are counterstained with neutral red.

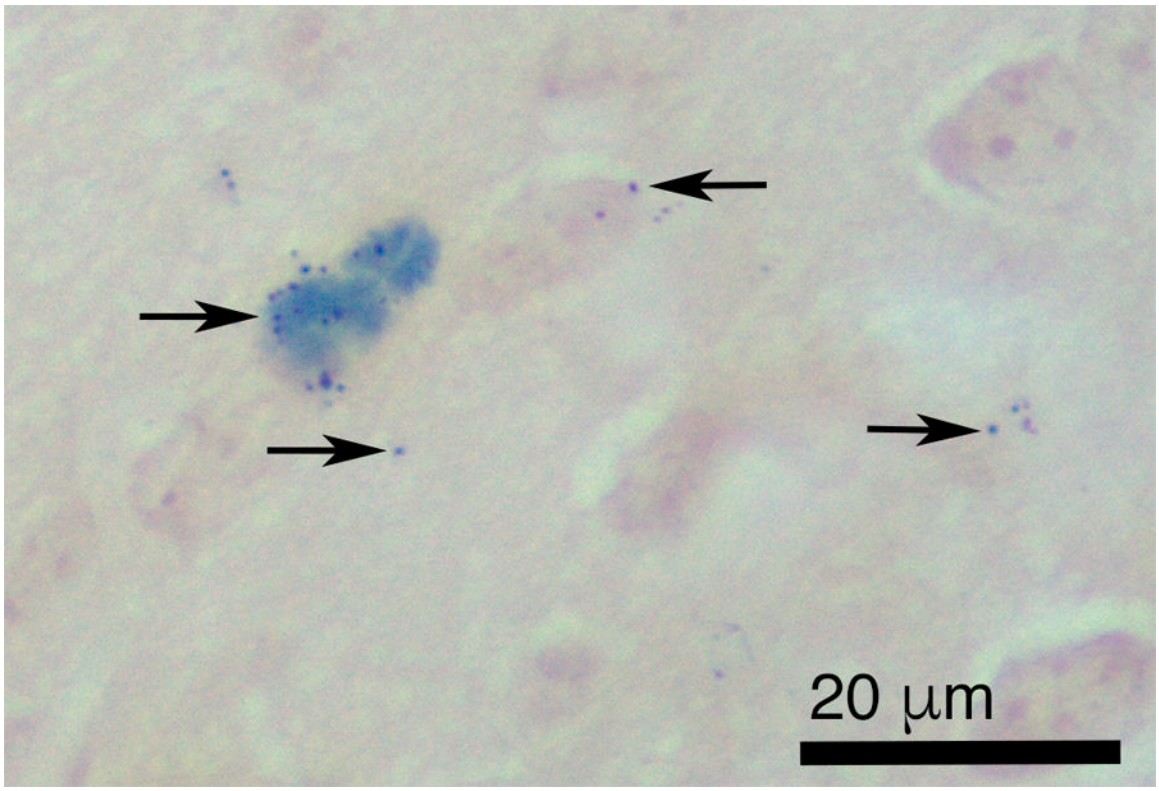

Figure 7.
Light micrograph of paraffin section of olfactory bulb from iron–soot exposed mice. Arrows indicate Prussian blue reaction product (deep blue precipitate) demonstrating the presence of ferric iron in the olfactory bulb. Neutral red counterstain.

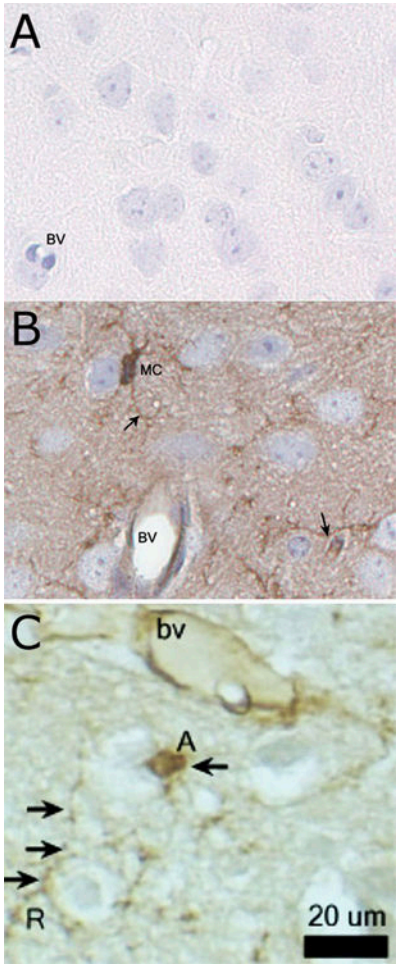

Figure 8.

Immunostaining of microglial cells of the olfactory bulb with Ricinus communis agglutinin (RCA-1) lectin. (A) The negative control with primary RCA-1 lectin antibody omitted. (B) Diffuse staining of RCA-1 lectin-positive cells with prominent microglial staining of the cell body (MC) and thin, elongated cytoplasmic processes extending beyond the cell nucleus (arrows). (C) An activated microglial cell (labeled A) exhibited a large, rounded nucleus and retraction of cytoplasmic processes, while resting microglial cells had small, elliptical nuclei and long, branched processes. Hematoxylin counterstain. BV ¼ blood vessel; MC ¼ microglial cells.

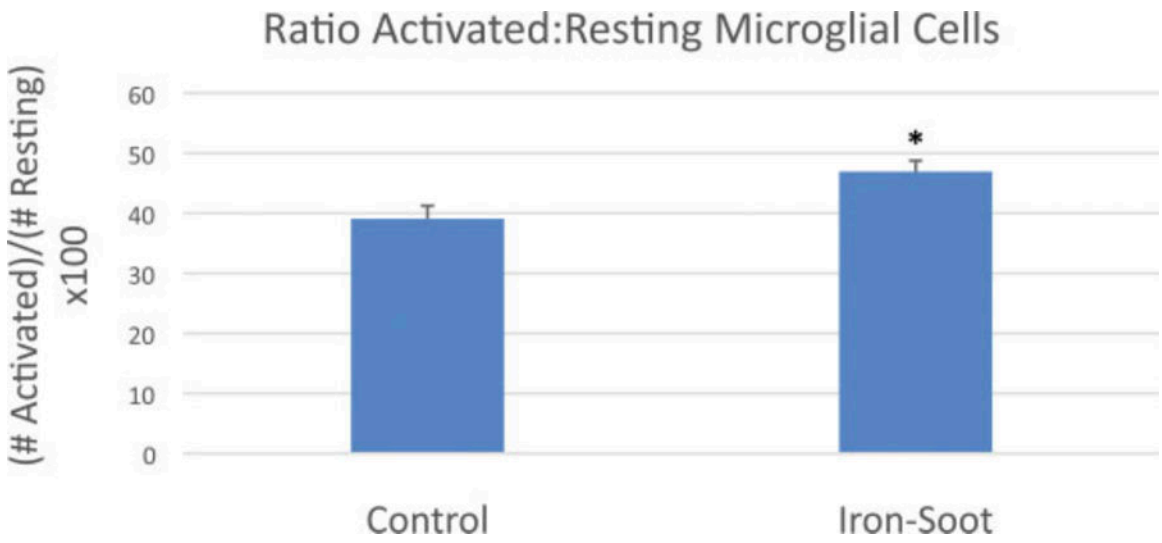

Figure 9.

Graph of total (resting þ activated) microglial cells for sham controls and animals exposed to iron–soot ultrafine particles. Two different levels of the olfactory bulb were analyzed at 20 magnification. Six nonoverlapping high power fields per level were analyzed for a total of 12 nonoverlapping fields. Six animals from each group were examined. Group means were 75.3 + 9.3 in sham controls and 81 + 20.8 in animals exposed to iron–soot nanoparticles. No statistical significance was achieved (p ¼ .25).

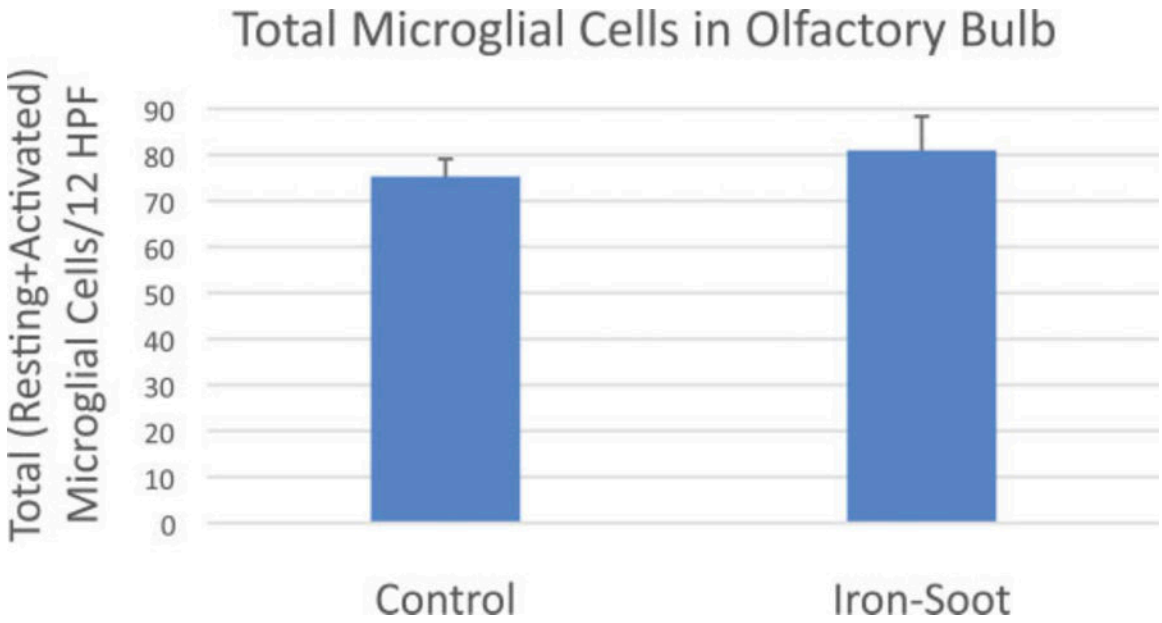

Figure 10.

The ratio of activated to resting microglial cells in the olfactory bulb of sham controls and animals exposed to iron–soot ultrafine particles. The ratio was 0.39 in sham controls and 0.47 in animals exposed to iron–soot ultrafine particles; there was a significant difference between groups (*p ¼ .045).

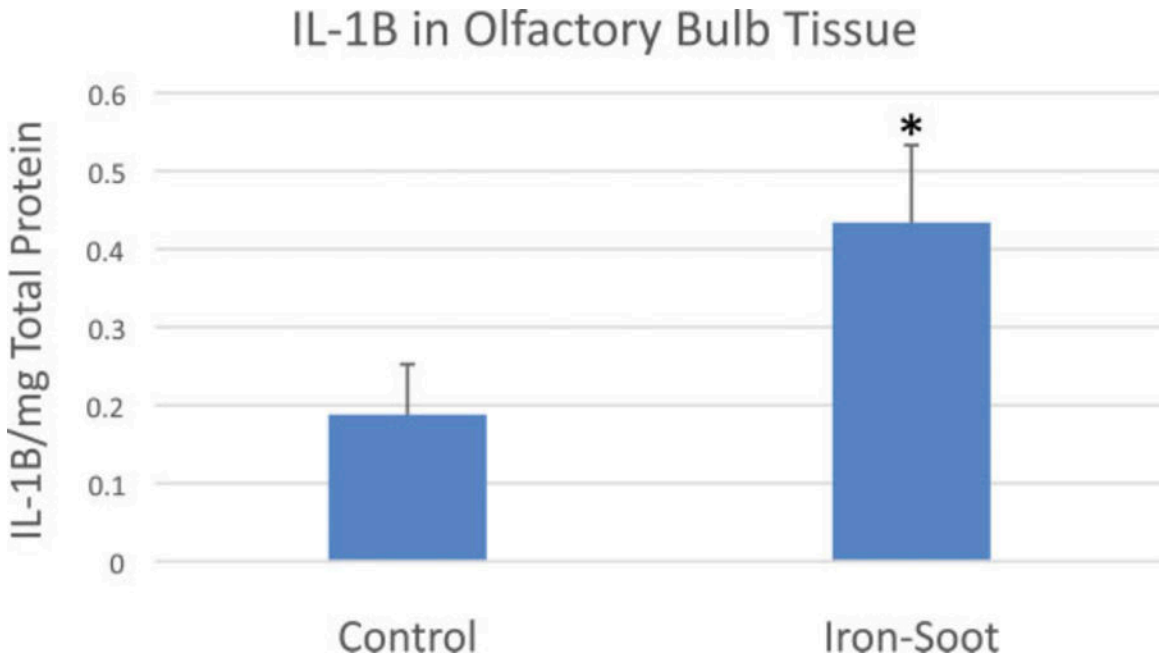

Figure 11.

IL-1b levels in the olfactory bulb for sham controls and animals exposed to iron–soot ultrafine particles. Group means were 0.19 + 0.11 pg/mg (control) and 0.43 + 0.24 pg/mg (iron–soot); a statistically significant difference was noted between groups (*p ¼ .038).